

FLUORESCENCE IMAGING USING TRANSPORT-THEORY-BASED IMAGING OPERATORS

Jenghwa Chang¹, Harry Graber², Raphael Aronson³, Randall L. Barbour^{1,2}

Department of Pathology¹ and Department of Physiology and Biophysics²,
SUNY Health Science Center at Brooklyn; Bioimaging Sciences Corporation³

Abstract

We derive a linear operator, based on transport theory, for imaging fluorophore concentrations. The elements of the weight matrix of the resulting system are calculated from results of Monte Carlo simulations. Experimental data were collected by irradiating a cylindrical phantom containing two fluorophore-filled balloons with laser light. The reconstruction results show that good quality images can be obtained, with both embedded objects accurately located.

1. INTRODUCTION

Optical imaging of physiological states using tomographic illumination and detection schemes has been studied for the past few years [1, 2]. In most cases, perturbation methods embodying either the Born or Rytov approximation are used for analysis of time-resolved, time-harmonic, or continuous-wave (CW) measurements, where difference signals between reference and perturbed media are obtained and used to reconstruct the change in the properties of the perturbed medium. The difference signal is usually very small and is sensitive to noise.

The use of fluorescent light for optical imaging has several important advantages. The fluorophore actively emits light, which can be much more precisely detected because the reference level is zero. A filter can be used to differentiate the emitted light from the excitation light to reduce contamination from the source. Finally, fluorescent probes can be tagged to antibodies to target tissues of interest selectively. The use of fluorescent probes has supplanted that of radioisotopes in some research and clinical laboratory procedures; we anticipate that fluorescence may also be used instead of radioactivity in techniques, such as PET and SPECT, designed for imaging thick tissue structures.

In this paper, we derive an imaging operator based on transport theory. The final form of this operator is a system of linear equations which can be easily solved by iterative methods. Monte Carlo simulations were performed to calculate this operator. Experimental data were collected using a CT-type scanning laser system. Image reconstructions were performed using projection onto convex sets (POCS), conjugate gradient descent (CGD), and simultaneous algebraic reconstruction technique (SART) methods.

2. THEORY

Light propagation in a material can be described by the radiative transport equation [3],

$$\frac{1}{c} \frac{\partial \phi}{\partial t} + \Omega \cdot \nabla \phi + \mu_T \phi = s + \int_0^\infty \int_{4\pi} \mu_s(\mathbf{r}, \Omega' \cdot \Omega, E' \rightarrow E) \phi' d\Omega' dE', \quad (1)$$

where c is the speed of light, E is the energy of the photon, $d\Omega$ is the differential solid angle, $\phi = \phi(\mathbf{r}, \Omega, E, t)$ and $\phi' = \phi(\mathbf{r}', \Omega', E', t)$ are angular intensities, $s = s(\mathbf{r}, \Omega, E, t)$ is the angular source intensity, $\mu_s(\mathbf{r}, \Omega' \cdot \Omega, E' \rightarrow E)$ is the macroscopic differential scattering cross section, and $\mu_T = \mu_T(\mathbf{r}, E)$ is the macroscopic total cross section. In this study, we assume that the excitation and emitted light are monoenergetic with energies E_1 and E_2 , respectively. Then (1) reduces to two coupled equations. For the excitation intensity,

$$\frac{1}{c} \frac{\partial \phi_1}{\partial t} + \Omega \cdot \nabla \phi_1 + (\mu_{T,1} + \mu_{T,1 \rightarrow 2}) \phi_1 = s_1 + \int_{4\pi} \mu_{s,1}(\Omega' \cdot \Omega) \phi_1' d\Omega', \quad (2)$$

where $\mu_{T,1}$ is the total cross section of the reference medium for E_1 , and $\mu_{T,1 \rightarrow 2}$ is the change in total cross section after the fluorophore is added. For the fluorescence intensity,

$$\begin{aligned} & \frac{1}{c} \frac{\partial \phi_2}{\partial t} + \Omega \cdot \nabla \phi_2 + \mu_{T,2} \phi_2 \\ &= \frac{\gamma \mu_{T,1 \rightarrow 2}}{4\pi\tau} H(t) e^{-\frac{t}{\tau}} \otimes \phi_1 + \int_{4\pi} \mu_{s,2}(\Omega' \cdot \Omega) \phi_2' d\Omega' \quad (3) \\ &= s_2 + \int_{4\pi} \mu_{s,2}(\Omega' \cdot \Omega) \phi_2' d\Omega', \end{aligned}$$

where \otimes indicates a convolution in time, γ is the quantum efficiency, τ is the mean lifetime of the fluorescent probe's excited state, and $H(t)$ is the Heaviside step function. Let R be the reading of a given detector for the emitted intensity, and $r = r_2(\mathbf{r}, \Omega, E, t)$ be the detector sensitivity function. Then

$$\begin{aligned} R &= \int_{V'} \int_{4\pi} r_2 \otimes \left(\int_{V'} \int_{4\pi} s_2' \otimes G_2(\mathbf{r}, \Omega; \mathbf{r}', \Omega'; t) d\Omega' d^3r' \right) d\Omega d^3r \\ &= \int_{V'} \int_{4\pi} s_2' \otimes \left(\int_{V'} \int_{4\pi} r_2 \otimes G_2(\mathbf{r}', -\Omega'; \mathbf{r}, -\Omega; t) d\Omega d^3r \right) d\Omega' d^3r' \quad (4) \\ &= \int_{V'} \int_{4\pi} \frac{\gamma \mu_{T,1 \rightarrow 2}}{4\pi\tau} H(t) e^{-\frac{t}{\tau}} \otimes \phi_1 \otimes \phi_2' d\Omega d^3r = \int_{V'} w_2 \mu_{T,1 \rightarrow 2} d^3r, \end{aligned}$$

where

$G_2(\mathbf{r}, \Omega; \mathbf{r}', \Omega'; t) =$ Green's function at \mathbf{r} and direction Ω , with source located at \mathbf{r}' and direction Ω' ,

$$\phi_2^+ = \int_V \int_{4\pi} r_2' \otimes G_2(\mathbf{r}, -\Omega; \mathbf{r}', -\Omega'; t) d\Omega' d^3 r',$$

$$w_2 = \int_{4\pi} \frac{\gamma}{4\pi\tau} H(t) e^{-\frac{t}{\tau}} \otimes \phi_1 \otimes \phi_2^+ d\Omega.$$

If we assume that $\mu_{T,1 \rightarrow 2} \ll \mu_{T,1}$, the solution to (2) can be approximated by the solution when $\mu_{T,1 \rightarrow 2}$ is not present. Then the *weight function* w_2 can be calculated and $\mu_{T,1 \rightarrow 2}$ can be imaged. For CW sources, the Fourier transform of (4) may be computed, and the corresponding weight function is

$$\begin{aligned} \tilde{\phi}_2'^+ &= \int_V \int_{4\pi} \tilde{r}_2' \tilde{G}_2(\mathbf{r}', -\Omega'; \mathbf{r}, -\Omega; 0) d\Omega d^3 r, \\ \tilde{w}_2 &= \int_{4\pi} \frac{\gamma}{4\pi} \tilde{\phi}_1 \tilde{\phi}_2'^+ d\Omega, \end{aligned} \quad (5)$$

where ‘ $\tilde{}$ ’ denotes a Fourier transform. Eqs. (4) and (5) can be discretized. The discretized version can be written in matrix form as

$$\mathbf{W}\boldsymbol{\mu} = \mathbf{R}. \quad (6)$$

3. EXPERIMENT AND IMAGE RECONSTRUCTION

Figure 1 illustrates the experimental setup for this study. Balloons filled with Rhodamine 6G dye at a concentration of $\sim 52 \mu\text{M}$ were embedded in a 8 cm diameter cylindrical phantom filled with 0.2% Intralipid® (% lipid per unit volume). The masses of the balloons were 0.84g and 1.02g. A 0.75W, multi-line (average wavelength $\sim 490 \text{ nm}$) argon laser irradiated the phantom and fluorescent light (max. emission at $\sim 560 \text{ nm}$) was collected on the boundary. A filter blocked excitation light from entering the detector. The diameter of the phantom was ~ 20 mean free pathlengths for the excitation light. A Monte Carlo simulation was performed for phantoms of the same optical thickness to get the direct and adjoint solutions for weight function calculation. Image reconstructions were performed using three iterative algorithms — POCS, CGD, and SART — with a rescaling technique and positivity constraints [4].

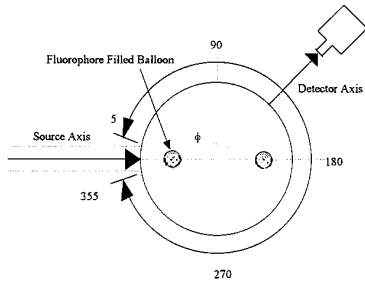


Figure 1. Experimental setup for this study.

4. RESULTS AND DISCUSSION

Figure 2 illustrates the reconstruction results after 10 and 10,000 iterations, using all three reconstruction algorithms. All methods produce good images after 10,000 iterations, with the two fluorescent balloons separated and accurately located. Resolution is evident in the POCS and CGD results after 10 iterations. Artifacts are observable near the boundary in all reconstructions. POCS produces the lowest amount of noise while the SART produce the most artifacts.

These results demonstrate that the imaging method presented here can successfully resolve multiple fluorescent objects. The location, size and volume difference of the objects were clearly identified, and sharp edge detection was achieved.

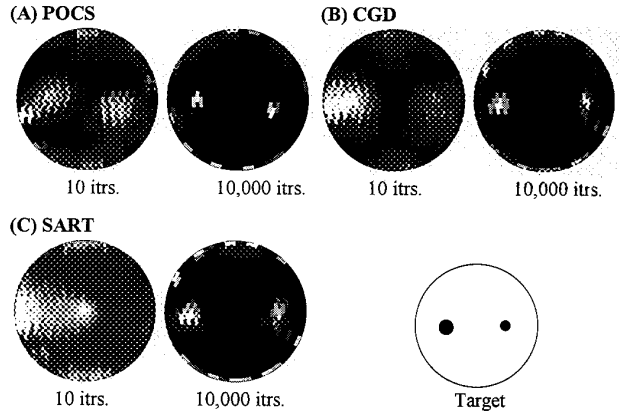


Figure 2. Reconstruction of the fluorescent images after 10, and 10,000 iterations. (A) POCS, (B) CGD, (C) SART.

ACKNOWLEDGMENT

This work was supported in part by NIH grant R01 CA59955, by ONR grant 00149510063, and by the New York State Science and Technology Foundation.

REFERENCES

- [1] *Medical Optical Tomography: Functional Imaging and Monitoring*, G. Müller *et al.*, eds., SPIE Institutes vol. IS11, SPIE Press, Bellingham, WA, 1993.
- [2] *OSA Proceedings on Advances in Optical Imaging and Photon Migration*, R. R. Alfano, ed., vol. 21., Optical Society of America, Washington, DC, 1994.
- [3] NCRP Scientific Committee 52, *Conceptual Basis for Calculations of Absorbed-Dose Distribution*, NCRP Report No. 108, 1991.
- [4] J. Chang, H. L. Graber, R. L. Barbour, "Image reconstruction of dense scattering media from CW sources using constrained CGD and a matrix rescaling technique," in *Proc. Optical Tomography, Photon Migration, and Spectroscopy of Tissue and Model Media: Theory, Human Studies, and Instrumentation*, vol. SPIE-2389, (San Jose), Feb. 1995.